

## **Structural basis of the differential binding of engineered knottins to integrins $\alpha V\beta 3$ and $\alpha 5\beta 1$**

Johannes F. Van Agthoven<sup>1,2,3</sup>, Hengameh Shams<sup>4</sup>, Frank V. Cochran<sup>5</sup>, José L. Alonso<sup>1,2,3</sup>, James R. Kintzing<sup>5</sup>, Kiavash Garakani<sup>4</sup>, Brian D. Adair<sup>1,2,3</sup>, Jian-Ping Xiong<sup>1,2,3</sup>, Mohammad R. K. Mofrad<sup>4</sup>, Jennifer R. Cochran<sup>5</sup> and M. Amin Arnaout<sup>1,2,3\*</sup>

From the <sup>1</sup>Leukocyte Biology and Inflammation Program, <sup>2</sup>Structural Biology Program, <sup>3</sup>Division of Nephrology/Department of Medicine, Massachusetts General Hospital and Harvard Medical School, Charlestown, MA, 02129, USA; <sup>4</sup> Departments of Bioengineering and Mechanical Engineering, University of California, Berkeley, CA, 94720, USA. <sup>5</sup> Departments of Bioengineering and Chemical Engineering, Stanford University, Stanford, CA, 94305, USA.

\* Lead and corresponding author: EM: [aarnaout1@mgh.harvard.edu](mailto:aarnaout1@mgh.harvard.edu)

## Summary

Targeting both integrins  $\alpha V\beta 3$  and  $\alpha 5\beta 1$  simultaneously appears to be more effective in cancer therapy than targeting each one alone. The structural requirements for bispecific binding of ligand to integrins has not been fully elucidated. RGD-containing knottin 2.5F binds selectively to  $\alpha V\beta 3$  and  $\alpha 5\beta 1$ , whereas knottin 2.5D is  $\alpha V\beta 3$ -specific. To elucidate the structural basis of this selectivity, we determined the structures of 2.5F and 2.5D as apo-proteins and in complex with  $\alpha V\beta 3$ , and compared their interactions with integrins using molecular dynamics simulations. These studies show that 2.5D engages  $\alpha V\beta 3$  by an induced fit, but conformational selection of a flexible RGD loop accounts for high affinity selective binding of 2.5F to both integrins. The contrasting binding of the highly flexible low affinity linear RGD peptides to multiple integrins, suggests that a "Goldilocks zone" of conformational flexibility of the RGD loop in 2.5F underlies its selective binding promiscuity to integrins.

## Keywords:

Keywords: Integrins, Receptors/Structure-Function, Protein crystallography, NMR, Molecular dynamics, Cancer therapy.

## Introduction

Heterodimeric  $\alpha/\beta$  integrins comprise a large family of divalent cation-dependent adhesion receptors that mediate cell-cell and cell-matrix interactions, which underlie their essential roles in normal metazoan physiology but also in contributing to many diseases including pathologic thrombosis, inflammation, autoimmunity and cancer (Raab-Westphal et al., 2017). In response to cell-activating stimuli, intracellular signals are generated that rapidly convert integrins into a ligand-competent state, a process termed inside-out signaling (Arnaout et al., 2007). Physiologic ligands, prototyped by the Arg-Gly-Asp (RGD) sequence motif, then bind the integrin head (formed of the  $\alpha$ -subunit propeller and  $\beta$ -subunit  $\beta A$  domains) (Xiong et al., 2002). A carboxylate group of the ligand Asp makes an electrostatic contact with a  $Mg^{2+}$  ion coordinated at a *metal-ion-dependent adhesion site* (MIDAS) of the  $\beta A$  domain, and the ligand Arg inserts into a pocket in the  $\alpha$ -subunit propeller. Ligand binding induces tertiary changes in  $\beta A$  that are converted to quaternary changes in the ectodomain, thus forging links of the integrin cytoplasmic tails with the actin cytoskeleton to regulate cell function, a process termed outside-in signaling (Friedland et al., 2009).

Therapeutic targeting of integrins has generally focused on development of peptides or small molecules that primarily target a single integrin (Kapp et al., 2017), an approach that has been effective in platelets, where integrin  $\alpha IIb\beta 3$  is most abundant (Coller and Shattil, 2008). However, in other cell types expressing multiple integrins, high selectivity for a single integrin may promote upregulation of another integrin sharing the same ligand, leading to reduced effectiveness, drug resistance, or even paradoxical effects. This scenario may be particularly relevant in cancer cells, where primary targeting of  $\alpha V\beta 3$  with cilengitide failed to prolong survival of patients with glioblastoma (Mason, 2015), likely related to unfavorable pharmacokinetics, enhanced  $\alpha 5\beta 1$ -mediated cell migration (Caswell et al., 2008; Christoforides et al., 2012) and agonist-like behavior (Reynolds et al., 2009). Recent studies also showed

superiority of targeting  $\alpha V\beta 3$  plus  $\alpha 5\beta 1$  as compared to  $\alpha V\beta 3$  alone in noninvasive *in vivo* imaging of brain cancer in mice (Moore et al., 2013).

The engineered 3.5kDa miniproteins knottins 2.5D and 2.5F bind with nanomolar affinity to  $\alpha V\beta 3$  (2.5D) or to both  $\alpha V\beta 3$  and  $\alpha 5\beta 1$  (2.5F) (Kimura et al., 2009a). 2.5D and 2.5F only differ in four residues: two on either side of the RGD motif (Figure 1A). In this report, we determined the solution structures of 2.5F and 2.5D and their crystal structures in complex with  $\alpha V\beta 3$ . Our results show that the 2.5F and 2.5D use different binding modes to interact with  $\alpha V\beta 3$  that are critically dependent on the degree of conformational flexibility of the respective RGD loop backbone. These data suggest that flexibility of the RGD loop in 2.5F is just sufficient to allow it to bind both integrins by adopting conformations to fit both binding sites but not so large, as in linear RGD peptides, that the entropic cost of stabilizing the loop in a single conformation will compromise its high-affinity binding.

## Results

**Integrin binding to 2.5D and 2.5F.** We measured binding of 2.5D-Fc or 2.5F-Fc fusion proteins to K562 cells stably expressing recombinant  $\alpha V\beta 3$  ( $\alpha V\beta 3$ -K562) and to K562 cells, which constitutively express  $\alpha 5\beta 1$  integrin. 2.5D bound to  $\alpha V\beta 3$ -K562 cells with nanomolar affinity ( $1.4 \pm 0.4$  nM, Figure 1B, D), but exhibited no measurable binding affinity to K562 cells (Figure 1B, D), over the same range, as was also true for the scrambled knottin FN-RDG2 (where the RGD motif is replaced with RDG (Kimura et al., 2009b)). In contrast, 2.5F bound both  $\alpha V\beta 3$ -K562 and K562 with similar affinities ( $6.9 \pm 1.3$  nM and  $9.2 \pm 1.4$  nM, respectively) (Figure 1C, D). Both 2.5D and 2.5F also bound U87MG glioblastoma cells ( $1.7 \pm 0.6$  nM and  $5.9 \pm 1.3$  nM, respectively) (Figure 1B- D), which express high levels of  $\alpha V\beta 3$  (Dumont et al., 2009).

**NMR structures of 2.5D and 2.5F.** To begin to elucidate the structural basis for selectivity of knottin/integrin binding, we first determined the solution structures of 2.5D and 2.5F by NMR (Table 1). As expected, both knottins assumed the same compact structure held together by three disulfide bonds, typical of the cysteine inhibitor family (Figure 2A, B). However, structure of the engineered RGD-containing loop flanked by prolines 3 and 11 was drastically different in the two knottins (Figure 2A, B). In 2.5D, this loop maintains a nearly single packed conformation (Figure 2A, C, D), but is flexible in 2.5F (Figure 2B-D).

**X-ray structures of integrin-bound 2.5D and 2.5F.** Knottins 2.5D and 2.5F were each soaked into preformed  $\alpha V\beta 3$  ectodomain crystals in presence of 1 mM  $Mn^{2+}$  and the crystal structure of the respective complex was determined as previously described (Van Agthoven et al., 2014; Xiong et al., 2002). Simulated annealing composite omit maps showed clear ligand density, and allowed complete tracing of the knottin macromolecule (Figure 3, Table 2, Figure S1) with Real Space Cross Correlations (RSCCs) for RGD in both knottins of 0.93-0.97, suggesting almost full occupancy of the ligand. The RGD motif of each ligand inserts into the crevice between the propeller and  $\beta A$  domains and contacts both in an identical manner (Figure 3A-F). The Arg<sup>6</sup> guanidinium of each knottin contacts  $\alpha V$ -Asp<sup>218</sup> of the propeller, with a carboxylate from Asp<sup>8</sup> contacting the MIDAS  $Mn^{2+}$ . In the  $\alpha V\beta 3$ /2.5D structure, 2.5D residues Ala<sup>10</sup>, Pro<sup>11</sup>, Pro<sup>28</sup>, Asn<sup>29</sup> and Phe<sup>31</sup> form additional van der Waals contacts with  $\beta A$  (Figure 3G). In the  $\alpha V\beta 3$ /2.5F structure, 2.5F-Arg<sup>4</sup> hydrogen bonds  $\beta A$ -Asn<sup>313</sup> and contacts the ADMIDAS metal ion indirectly through a chloride ion (Figure 3F). Other interactions include van der Waals contacts of 2.5F

residue Pro<sup>10</sup>, Pro<sup>11</sup>, and Phe<sup>31</sup> with  $\beta$ A (Figure 3H). These interactions, which bury a surface area of 654.6 Å<sup>2</sup> for  $\alpha$ V $\beta$ 3/2.5F and 606.2 Å<sup>2</sup> for  $\alpha$ V $\beta$ 3/2.5D structures account for the high affinity binding of each ligand to  $\alpha$ V $\beta$ 3.

As with binding of the natural ligand FN10 or the partial agonist cilengitide to  $\alpha$ V $\beta$ 3 (Van Agthoven et al., 2014; Xiong et al., 2002), binding of 2.5D or 2.5F induced a 3.7Å inward movement of the  $\alpha$ 1 helix of the  $\beta$ A domain towards the MIDAS Mn<sup>2+</sup>, and restructuring of the F/ $\alpha$ 7 loop (Figure S2A), confirming that both knottins are partial agonists. The shape of the CD loop of the  $\beta$ TD in both knottin/integrin structures was also comparable to the one published for  $\alpha$ V $\beta$ 3/wtFN10 (Van Agthoven et al., 2014) (Figure S2B-D). However, whereas the crystal structure of the pure antagonist hFN10 bound to  $\alpha$ V $\beta$ 3 showed a h-bond between  $\beta$ 3-Glu<sup>319</sup> of  $\beta$ A and  $\beta$ 3-Ser<sup>674</sup> of  $\beta$ TD and a visible glycan at Asn<sup>711</sup>, both features were absent in the  $\alpha$ V $\beta$ 3/2.5F and  $\alpha$ V $\beta$ 3/2.5D structures (Figure S2B-D).

**Conformations of the RGD-containing loops of 2.5D and 2.5F bound to  $\alpha$ V $\beta$ 3.** In contrast to the major differences in conformation of the RGD-containing loops of 2.5D and 2.5F (Figure 2), the two loops were largely superposable in the integrin-bound state (Figure 4A), with a root mean square deviation (r.m.s.d.) of 0.62±0.27Å<sup>2</sup> (mean±sd). Superposing the crystal structures of the integrin-bound loops on the respective NMR structure of the lowest energy state showed dramatic differences in the RGD-containing loop of 2.5D (Figure 4B). The r.m.s.d. of this loop in 2.5D between the integrin-bound and solution states is 3.52±1.01Å<sup>2</sup>, which is significantly higher than its narrow r.m.s.d. in solution that is maintained in all 20 conformers (0.67±0.22 Å<sup>2</sup>, Figure 2D, Figure S3). The apo-protein state is stabilized by a 4-residue type I  $\beta$ -turn spanning Arg<sup>6</sup> to Trp<sup>9</sup>, with hydrogen bonds involving the carbonyl oxygens and amide nitrogens of Trp<sup>9</sup> and Arg<sup>6</sup>, and maintains a distance of ~6.4 Å between the  $\beta$  carbons of Arg<sup>6</sup> and Asp<sup>8</sup> ( $C_{\beta-\beta}^{RD}$ )(Figure 4C). The importance of a Trp residue immediately after RGD in forming a  $\beta$ -turn was previously noted (Park et al., 2002). When 2.5D is bound to  $\alpha$ V $\beta$ 3, the  $\beta$ -turn unfolds, with Trp<sup>9</sup> moving from the solvent-exposed state to form an internal van der Waals bond with Gly<sup>5</sup> (Figure 4D), thus extending the  $C_{\beta-\beta}^{RD}$  distance to 9Å (Figure 4E). In contrast, the r.m.s.d. of the RGD-containing loop of 2.5F between the bound and solution structure is 3.13±1.64Å<sup>2</sup>, comparable to its r.m.s.d. in solution (2.76±1.0 Å<sup>2</sup>) (Figure 4F), with conformational flexibility of the RGD loop backbone reflected in  $C_{\beta-\beta}^{RD}$  varying from 4.1Å in the lowest energy state to 8.8Å in conformer #14 (Figure 4G, Figure S3) that approaches the 9.1Å  $C_{\beta-\beta}^{RD}$  found in  $\alpha$ V $\beta$ 3/2.5F (Figure 4H) or RGD-bound  $\alpha$ 5 $\beta$ 1 ( $C_{\beta-\beta}^{RD}$ =8.8Å) structures (Figure 4 I).

**MD simulations of knottin binding to  $\alpha$ V $\beta$ 3 and  $\alpha$ 5 $\beta$ 1.** MD simulation was used to characterize the early stages in binding of 2.5F and 2.5D to  $\alpha$ V $\beta$ 3 and  $\alpha$ 5 $\beta$ 1. The lowest energy NMR structures of 2.5F and 2.5D were docked onto the  $\alpha$ V $\beta$ 3 and  $\alpha$ 5 $\beta$ 1 crystal structures, resulting in four protein complexes. In each complex, the knottin was moved 9Å away from the integrin surface allowing several water layers to form between the two before simulation was initiated. Over a 500-ns run, 2.5F associated with both  $\alpha$ V $\beta$ 3 (135±37 kcal/mole) and  $\alpha$ 5 $\beta$ 1 (81±51 kcal/mole) (Figure 5A, B, Supplemental Movies 1 and 2), recapitulating the cell-based data (Figure 1 B-D). The first dual contact of 2.5F with  $\alpha$ V $\beta$ 3 was detected at 0.02 ns of simulation by 2.5F-Arg<sup>6</sup> hydrogen-bonding  $\beta$ 3-Thr<sup>212</sup> and salt-bridging  $\beta$ 3-Asp<sup>150</sup>, and 2.5F-Asp<sup>8</sup> salt-bridging  $\beta$ 3-Arg<sup>214</sup> (Fig 5C). The first dual contact of 2.5F with  $\alpha$ 5 $\beta$ 1 was detected at 0.35

ns, but the interaction stabilized at 1.25 ns through a salt-bridge between 2.5F-Asp<sup>8</sup> and  $\beta$ 1-Lys<sup>182</sup> (Fig 5D).

As expected, 2.5D also bound  $\alpha$ V $\beta$ 3 effectively (164 $\pm$ 37 kcal/mole) (Figure 5A, B, Supplemental Movie 3). The low energy of interaction between 2.5D-Trp<sup>9</sup> and 2.5D-Gly<sup>5</sup> suggested that surrounding residues in the binding pocket of  $\alpha$ V $\beta$ 3 are involved in the conformational switch of 2.5D-Trp<sup>9</sup> from the solvent to the buried state. Consistently, over the course of the  $\alpha$ V $\beta$ 3/2.5D simulation, 2.5D-Trp<sup>9</sup> first formed an S- $\pi$  bond with  $\beta$ 3-Met<sup>180</sup> at 0.38 ns after the start of simulation, which was reinforced at 0.96 ns via an electrostatic interaction between 2.5D-Asp<sup>8</sup> and  $\beta$ 3-Arg<sup>214</sup> (Figure 5E). In contrast 2.5D rapidly diffused away from  $\alpha$ 5 $\beta$ 1 after 1.1 ns of interaction (7 $\pm$ 19 kcal/mole) (Figure 5A, B), unable to sustain the initial binding of 2.5D-Arg<sup>6</sup> to  $\beta$ 1-Gln<sup>221</sup> and  $\beta$ 1-Asp<sup>227</sup> at 0.01 ns (not shown) with additional contacts to the integrin (Figure 5F, Supplemental Movie 4).

**Binding of 2.5D and 2.5F to native and mutant cellular  $\alpha$ V $\beta$ 3.** To assess the contribution of the early contacts of 2.5D makes with  $\alpha$ V $\beta$ 3 on binding energy (Figure 5E), we replaced  $\beta$ 3-Met<sup>180</sup> with alanine ( $\beta$ 3-Met<sup>180</sup> has no homolog in  $\beta$ 1) and  $\beta$ 3-Arg<sup>214</sup> with glycine (the equivalent residue in  $\beta$ 1). MD simulations showed that the Met<sup>180</sup>/Arg<sup>214</sup>-Ala-Gly  $\alpha$ V $\beta$ 3 mutant ( $\alpha$ V $\beta$ 3<sup>\*\*</sup>) sustained a significant loss in binding energy (25 $\pm$ 19%) to 2.5D, but maintained the energy of interaction (111 $\pm$ 19%) with 2.5F (Figure 6A, B). To validate the MD data, we quantified the binding of Alexa-647-labeled 2.5F and 2.5D to wild-type  $\alpha$ V $\beta$ 3 and  $\alpha$ V $\beta$ 3<sup>\*\*</sup>, each transiently expressed in HEK293 cells. The double mutation reduced surface expression of  $\alpha$ V $\beta$ 3<sup>\*\*</sup> by ~50% compared to wild-type  $\alpha$ V $\beta$ 3 (Figure 6C). When binding of each labeled ligand to the integrin was corrected for the degree of receptor expression, binding of 2.5F to  $\alpha$ V $\beta$ 3<sup>\*\*</sup> was minimally affected (85 $\pm$ 9% of binding to wt-  $\alpha$ V $\beta$ 3, Figure 6D), but binding of 2.5D to  $\alpha$ V $\beta$ 3<sup>\*\*</sup> was markedly reduced (28 $\pm$ 1% of binding to wt-  $\alpha$ V $\beta$ 3) (Figure 6E).

## Discussion

The present studies show that specific recognition of  $\alpha$ V $\beta$ 3 by 2.5D requires high structural plasticity of the RGD-containing loop, revealed by comparing the conformational changes in loop backbone in structures of the apo-protein and  $\alpha$ V $\beta$ 3/2.5D complex. These comparisons also reveal a pronounced induced fit binding mechanism upon complex formation with  $\alpha$ V $\beta$ 3, which also resembles the well-known interactions between antibodies and antigens (Wilson and Stanfield, 1994). These features were not observed in binding of 2.5F to  $\alpha$ V $\beta$ 3, where the RGD-containing loop of the apo-protein is flexible, with some conformers having a  $C_{\beta-\beta}^{RD}$  distance comparable to that found in the  $\alpha$ V $\beta$ 3-bound state, suggesting that 2.5F binds  $\alpha$ V $\beta$ 3 by conformation selection.

MD simulations elucidated the structural basis of the induced fit that underlies binding of 2.5D to  $\alpha$ V $\beta$ 3. The RGD-containing loop in the apo-protein is stabilized by a Type I  $\beta$ -turn, yielding a  $C_{\beta-\beta}^{RD}$  distance of ~6.4Å, which extends to the optimal 9Å distance as a result of the switch of 2.5D-Trp<sup>9</sup> from a solvent to a buried state. This switch appears to be driven by an early contacts with  $\beta$ 3-Met<sup>180</sup> and  $\beta$ 3-Arg<sup>214</sup>, and is later influenced by the surrounding hydrophilic environment ( $\beta$ 3-Tyr<sup>166</sup>,  $\beta$ 3-Arg<sup>214</sup>), as 2.5D-Asp<sup>8</sup> coordinates the metal ion at MIDAS. Substitution of  $\beta$ 3-Met<sup>180</sup> to Ala and  $\beta$ 3-Arg<sup>214</sup> to Gly (as in  $\beta$ 1) resulted in a major loss in

binding energy of 2.5D to  $\alpha V\beta 3$ . This was confirmed by assessing knottin binding to HEK293 transiently expressing wild-type  $\alpha V\beta 3$  or  $\alpha V\beta 3^{**}$ . Since  $\alpha 5\beta 1$  lacks the equivalent Met and Arg residues, the induced fit mechanism cannot proceed, accounting for the lack of binding of 2.5D to  $\alpha 5\beta 1$ . The  $C_{\beta-\beta}^{RD}$  distance offered by some conformers of the flexible RGD-containing loop in 2.5F also accounts for its high affinity binding to  $\alpha 5\beta 1$ .

The differences between 2.5F and 2.5D in adapting to the ligand-binding pocket in  $\alpha 5\beta 1$  likely relates to the RGD flanking residues of each ligand. Notably, 2.5F harbors two more prolines Pro<sup>5</sup> and Pro<sup>10</sup> in the RGD-containing loop (RP<sup>5</sup>RGDNP<sup>10</sup>P) when compared to that in 2.5D (QG<sup>5</sup>RGDWA<sup>10</sup>P)(Figure 1A)(Kimura et al., 2009b). These trans-isomers of the prolines likely introduce local rigidity through their pyrrolidine ring, limiting the backbone dihedral angle to  $\sim 90^\circ$ , thus restraining the RGD-containing loop from adopting a  $\beta$ -turn fold, as in 2.5D (Krieger et al., 2005; Pabon and Camacho, 2017). Previous studies showed that the highly flexible linear RGD peptides have low affinity and are not specific for a particular integrin (Ruoslahti and Pierschbacher, 1987). Decreasing structural flexibility of the RGD loop by cyclization favors high affinity binding to integrins (Bogdanowich-Knipp et al., 1999), as it decreases the entropy term of the Gibbs free energy. However, our study shows that rigidifying the RGD loop limits the ability of 2.5D to bind certain integrins. The critical proline residues in the RGD-containing loop of 2.5F achieves a fine equilibrium between stability and flexibility of the RGD loop enabling a focused motional freedom (Krieger et al., 2005; Pabon and Camacho, 2017), where the RGD loop in 2.5F is flexible enough to bind both  $\alpha V\beta 3$  and  $\alpha 5\beta 1$  without excessive entropic contribution, which would hamper high affinity binding.

Eight of the 24 known mammalian integrins including  $\alpha V\beta 3$  and  $\alpha 5\beta 1$  bind to an RGD motif present in a host of natural ligands (Takada et al., 2007). High affinity peptidomimetics or RGD-like small molecules targeting single integrins have been developed. However, most of these continue to have residual but significant affinity to other RGD-binding integrins, and the selectivity of newer versions of these ligand-mimetics have not yet been fully explored in cell-based systems and at the high concentrations likely needed *in vivo* (Kapp et al., 2017). Given the ability of cancer cells to utilize both  $\alpha V\beta 3$  and  $\alpha 5\beta 1$  integrins for growth and metastasis, small molecules with multispecificity have been developed for potential applications in cancer therapy (Hatley et al., 2018; Sheldrake and Patterson, 2014). Despite these successes, development of multifunctional small molecule integrin antagonists that maintain high affinity and suitable pharmacokinetic properties remains a challenge (Nero et al., 2014). The engineered knottin miniproteins 2.5D and 2.5F have a number of advantages over small molecules and short peptides including exceptional structural stability, high affinity, and specificity to tumor-associated integrins (Kimura et al., 2009b; Kwan et al., 2017). Their amenability to large-scale synthesis provides a manufacturing advantage over monoclonal antibodies. These features highlight knottins as promising candidates to bridge the gap between small molecule drugs and monoclonal antibodies.

**Acknowledgements.** This work was supported by NIH grants DK088327 and DK48549 (to MAA), DK101628 (to JVA), from the National Institutes of Diabetes, Digestive and Kidney diseases (NIDDK) of the National Institutes of Health; the Stanford Bio-X Interdisciplinary Initiatives Program, the Stanford Cancer Institute and the Stanford Maternal & Child Health Research Institute (JRC); National Science Foundation (NSF) grant CBET-0829205 (to

MRKM). This work used resources of the Extreme Science and Engineering Discovery Environment (XSEDE) awarded to MRKM, which is supported by the National Science Foundation (NSF) (grant ACI-1053575). JRK was supported by a National Science Foundation Graduate Research Fellowship and an ARCS Scholar Award.

**Author contribution.** JVA, JLA, JRK, BDA and JRC designed and performed the ligand-binding studies. FVC performed the NMR studies. JVA collected the x-ray diffraction data and refined the crystal structures with JPX. HS, KG and MRKM generated the molecular dynamic simulation data. All authors interpreted the data. MAA conceived and oversaw the project and wrote the manuscript with input from all authors.

### **Declaration of Interests**

JRC is a cofounder of xCella Biosciences and inventor on US patents (8,536,301; 9,913,878) related to knottins. The other authors declare no competing interests.

**Table 1. NMR structural statistics for 2.5D and 2.5F 20-conformer ensembles**

	<b>2.5D</b>	<b>2.5F</b>
PDB Code	2M7T	6MM4
NMR-derived restraints		
Interproton total	462	340
short-range, $ i-j  \leq 1$	248	223
medium-range, $1 <  i-j  < 5$	78	48
long-range, $ i-j  \geq 5$	136	69
Dihedral angles	32	35
Hydrogen bonds	16	16
Disulfide bonds	18	18
Ramachandran statistics		
Residues in		
most favored regions (%)	86.3	87.5
additional allowed regions (%)	13.7	11.4
generously allowed regions (%)	0.0	0.5
disallowed regions (%)	0.0	0.7
RMSD statistics (residues 1-33)		
Average backbone RMSD to mean (Å)	0.26 +/- 0.06	1.04 +/- 0.28
Average heavy atom RMSD to mean (Å)	0.48 +/- 0.09	1.52 +/- 0.3

**Table 2. Data collection and refinement statistics.**

<b>Data collection</b>	<b><math>\alpha</math>V<math>\beta</math>3/2.5D</b>	<b><math>\alpha</math>V<math>\beta</math>3/2.5F</b>
PDB Code	6MSL	6MSU
Beamline	ID19 at APS	ID19 at APS
Space group	P3 <sub>2</sub> 21	P3 <sub>2</sub> 21
Unit cell dimensions (Å, °)	$a=b=129.8, c=305.9;$ $\alpha=\beta=90, \gamma=120$	$a=b=129.9, c=305.9;$ $\alpha=\beta=90, \gamma=120$
Resolution range (Å)	50.0-3.1	50.0-3.1
Wavelength (Å)	0.97921	0.97921
Total reflections	1,919,957	945,125
Unique reflections	54,885 (5,389)*	54,732 (5,385)
Completeness	100 (100)	100 (100)
Redundancy	6.9 (7.0)	6.2 (6.3)
Molecules in asymmetric unit	1	1
Average $I/\sigma$	14.1 (1.7)	15.3 (2.0)
$R_{merge}$ (%)	14.9 (169.4)	12.7 (131.8)
$R_{meas}$ (%)	16.2 (183.2)	13.9 (143.9)
$R_{pim}$ (%)	6.2 (68.6)	5.5 (57.1)
Wilson $B$ -factor	65.6	62.7
cc1/2	0.97 (0.52)	0.98 (0.61)
<b>Refinement statistics</b>		
Resolution range (Å)	49.2-3.1	49.3-3.1
$R_{factor}$ (%)	22.7 (30.2)	22.9 (31.8)
$R_{free}$ (%)#	26.8 (29.2)	27.6 (34.6)
No. of atoms	13,132	13,158
Protein	12,713	12,714
Water	4	4
Mn <sup>2+</sup>	8	8
Glc-NAc	407	431
Chloride	0	1
Average $B$ -factor for all atoms (Å <sup>2</sup> )	62.3	61.4
r.m.s. deviations		
Bond lengths (Å)	0.007	0.010
Bond angles (°)	1.10	1.63
Ramachandran plot		
Most favored (%)	89.9	90.2
Allowed regions (%)	9.8	9.5
Outliers (%)	0.2	0.2
Clashscore (%)	8.8	8.1
Rotamer outliers (%)	0	0

\* Values in parentheses are for the highest resolution shell (0.1 Å)

#  $R_{free}$  was calculated with 5% of the data

## Main Figures and Legends

**Figure 1. Primary sequence and binding properties of knottins 2.5D and 2.5F.** (A) The primary structure of EETI-II and of the engineered knottins 2.5D and 2.5F, where the 6-residue trypsin-binding sequence (P<sup>3</sup>RILMR) in native knottin is replaced with an 11-residue sequence containing the RGD motif. (B, C) Dose-response curves showing binding of Fc fusions of 2.5D (B), 2.5F (C) or a scrambled (scr) knottin (B, C) to native integrins expressed on U87MG,  $\alpha$ V $\beta$ 3 expressed on transfected K562 cells ( $\alpha$ V $\beta$ 3-K562), and native  $\alpha$ 5 $\beta$ 1 on K562 cells. Points display the mean and standard deviation for triplicate determinations. (D) Equilibrium binding constant ( $K_d$ ) values from the binding data shown in B, C, along with the standard error derived from the fitted curves. The  $K_d$  value derived from the curve fit of 2.5D-Fc binding to K562 in Figure 1B is not reliable as determined by the P value for the parameter, and thus not reported in Fig.1D. nd, not determined.

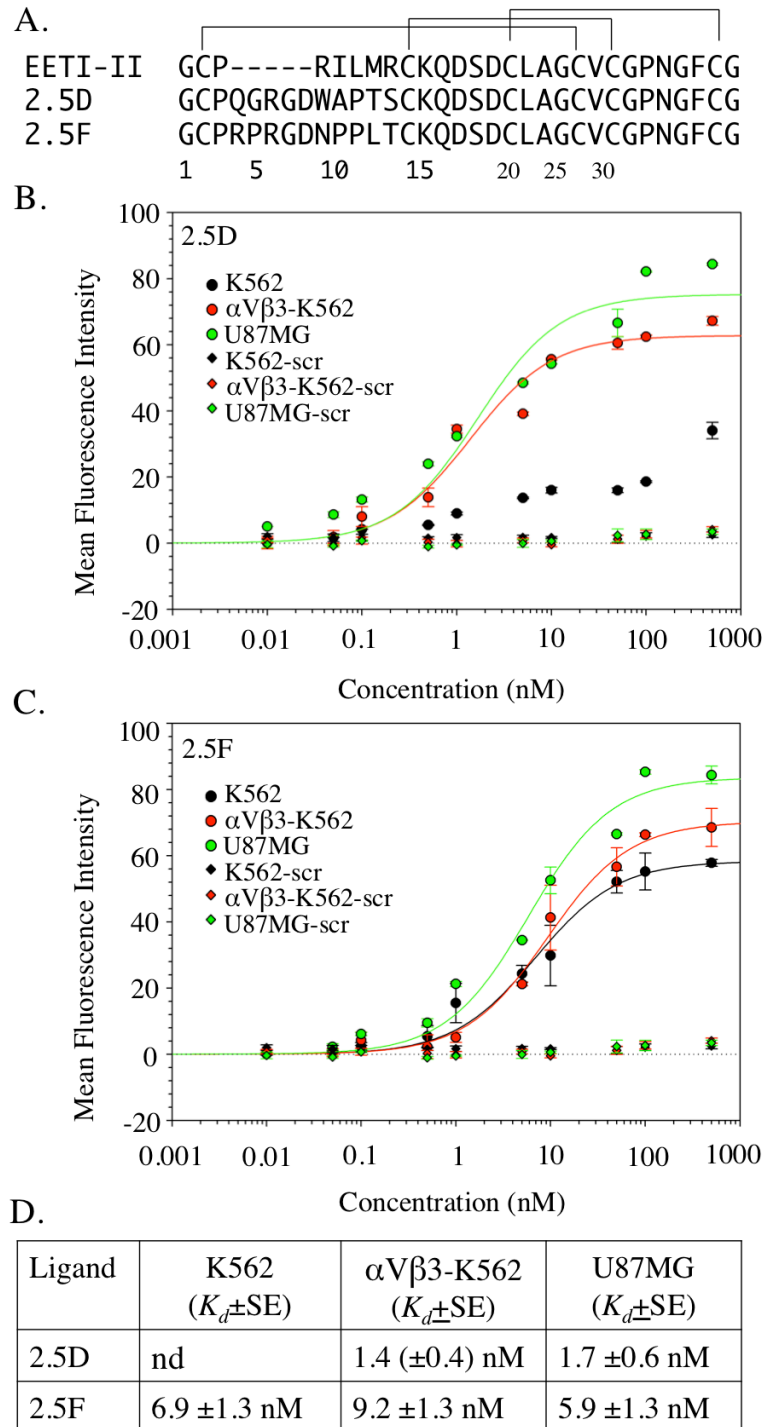
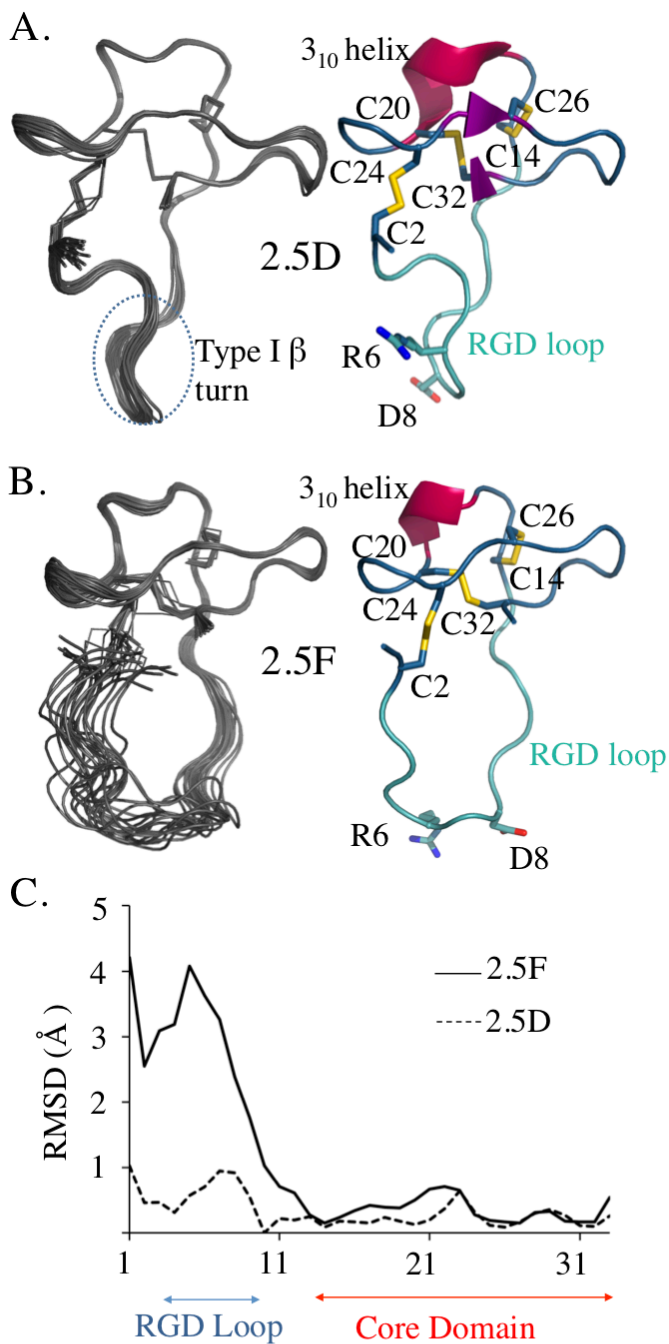


**Figure 2. NMR structures and analysis of 2.5D and 2.5F.**

(A, B) Solution NMR structures of knottins 2.5D (A) and 2.5F (B) represented as the 20 lowest energy conformers. Ribbon diagrams of the lowest energy conformer of 2.5D and 2.5F are shown to the right. The RGD loop is in cyan with the integrin RGD binding sequence in sticks. The core domain is blue with disulfide bonds in yellow sticks. The  $3_{10}$  helix is represented in red cartoon. (C) RMSD of solution structure of 2.5D and 2.5F plotted versus residue number. The RGD loop (residue 4-10) and core domain (residue 14-33) are indicated. (D) Table summarizing the RMSD values per domain shown as mean $\pm$ S.D.: core domain (residue 14-33) and RGD loop (residue 4-10).

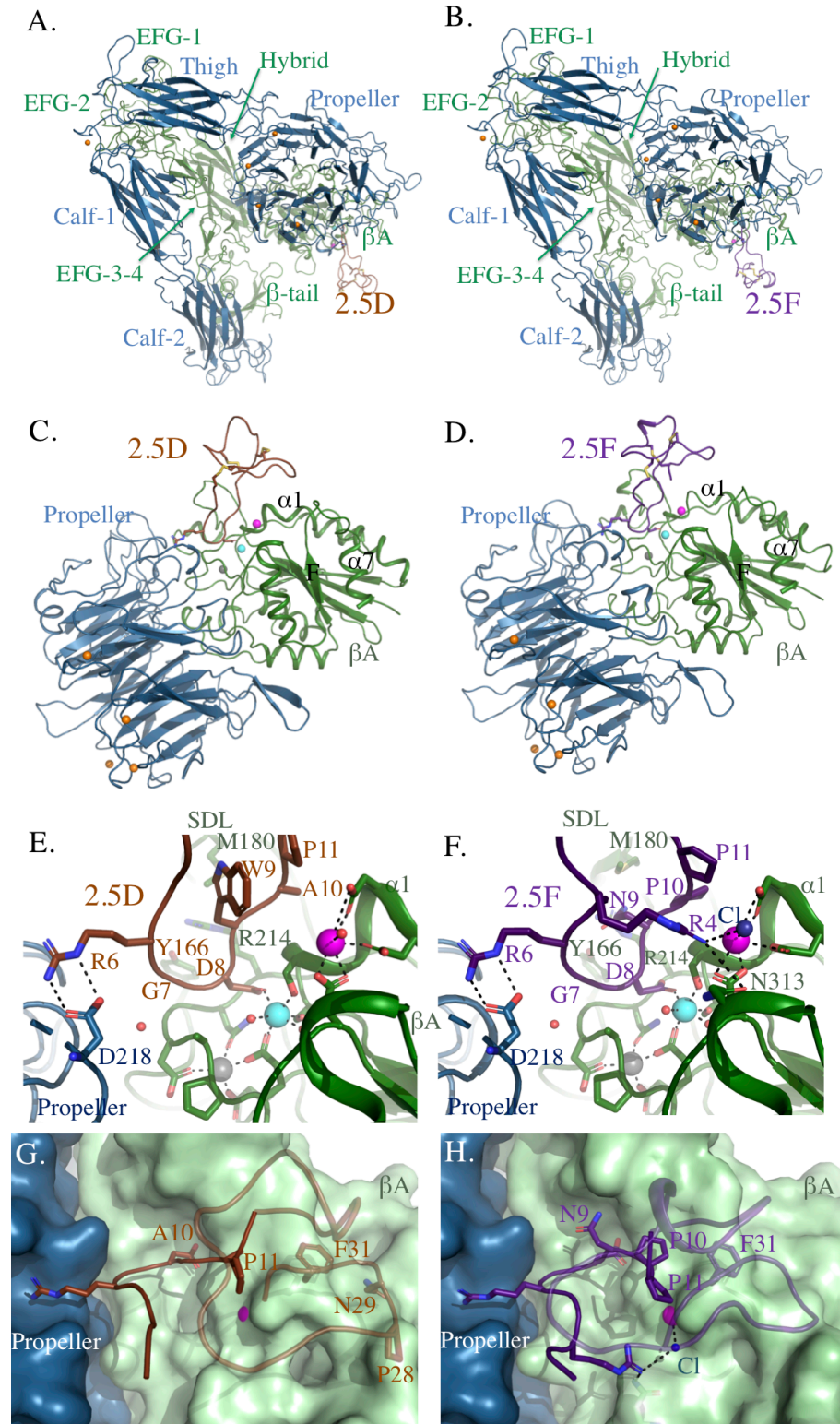


D.

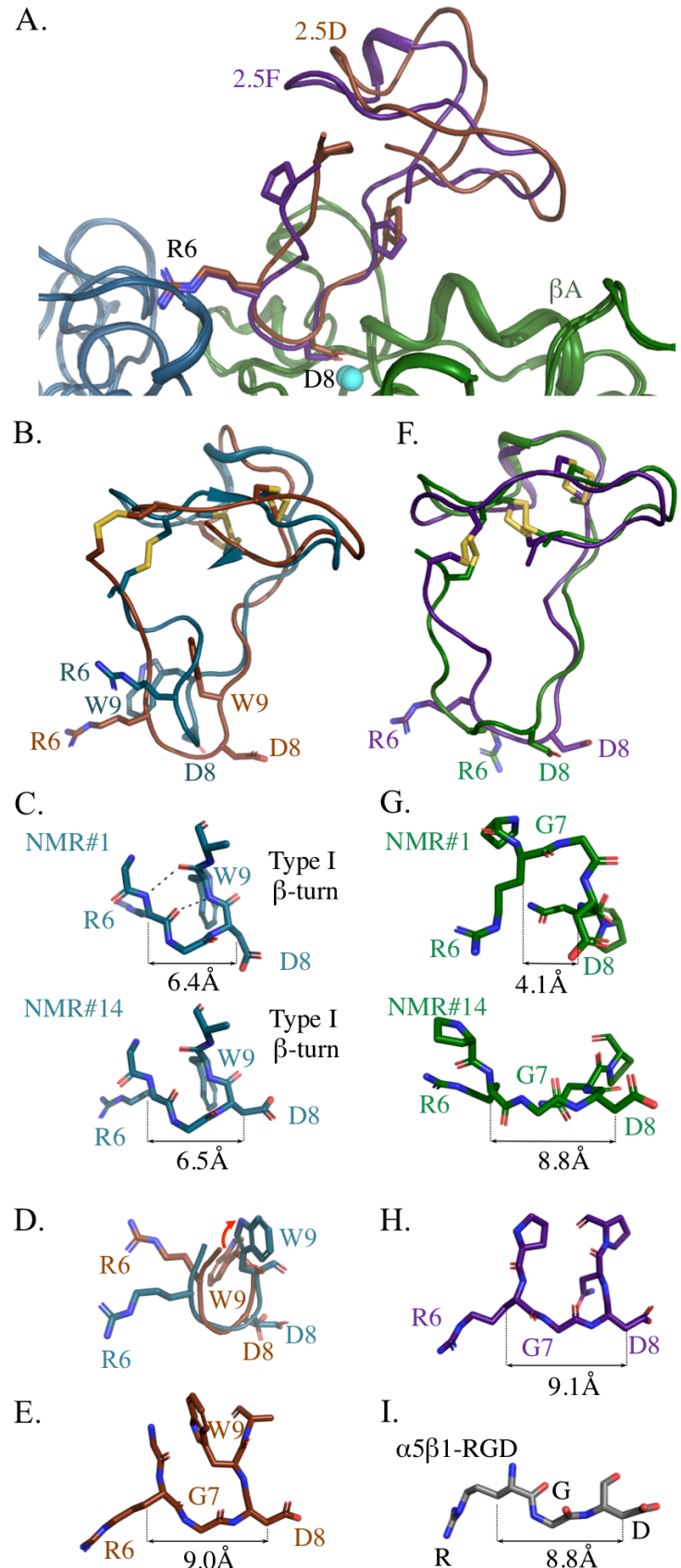
Ligand	RMSD RGD loop (4-10)	RMSD Core domain (14-33)	RMSD Overall
2.5F	2.76 Å ( $\pm$ 1.00)	0.35 Å ( $\pm$ 0.18)	1.14 Å ( $\pm$ 1.29)
2.5D	0.67 Å ( $\pm$ 0.22)	0.22 Å ( $\pm$ 0.12)	0.35 Å ( $\pm$ 0.26)

**Figure 3. Crystal structures of  $\alpha$ V $\beta$ 3 bound to knottins 2.5D or 2.5F.**

(A, B) Ribbon diagrams of  $\alpha$ V $\beta$ 3 ( $\alpha$ V is in blue and  $\beta$ 3 in green) bound to 2.5D (brown in A, C, E and G) or 2.5F (purple, in B, D, F and H). (C, D) Ribbon diagrams of the  $\alpha$ V $\beta$ 3 head bound to 2.5D (C) and 2.5F (D). The propeller is in blue and  $\beta$ A domain in green.  $Mn^{2+}$  ions at LIMBS (gray), MIDAS (cyan) and ADMIDAS (magenta) are shown as spheres (also in E-H). (E, F) Ribbon diagrams showing key electrostatic and hydrogen bond interactions and metal ion coordination in the structure of  $\alpha$ V $\beta$ 3/2.5D (E) and  $\alpha$ V $\beta$ 3/2.5F (F). 2.5F-R4 hydrogen bonds with  $\beta$ 3-N313. Additionally, 2.5F contacts the ADMIDAS ion through a chloride (Cl) ion represented as a blue sphere. Water molecules are shown as small red spheres. (G, H) Solvent accessible surface view of the integrin/ligand interface showing residues in 2.5D (A10, P11, P28, N29, and F31) and in 2.5F (N9, P10, P11 and F31) forming van der Waals ( $\leq 4\text{\AA}$ ) contacts with the  $\beta$ A domain. See also Figure S1 and S2.



**Figure 4. Structural comparisons of 2.5D and 2.5F in solution and integrin-bound.** (A) Ribbon diagram of the superposed crystal structures of 2.5D (brown) and 2.5F (purple) in the integrin bound state. (B, F) Crystal structures of 2.5D (brown) and 2.5F (purple) superimposed on lowest energy model #1 of apo 2.5D (B, tale) and apo 2.5F (F, green). (C, G) Stick diagrams of the RGD loop in apo 2.5D (tale) and apo 2.5F (green) of lowest energy NMR #1 and of NMR#14. The 2.5D apo structure shows a  $\beta$  hairpin Type I turn in the RGD loop. C $\beta$ -C $\beta$  distances is stable among 2.5D conformers but is variable in case of 2.5F. (D) Superposition of GRGDW (residues 5-9) of 2.5D in the apo (tale) and bound states (brown). The red arrow shows conformational change of 2.5D-W9 from solvent-exposed state in the apo form to buried state in the crystal structure. (E, H) Crystal structures of the integrin-bound RGD loops of 2.5D (E) and 2.5F (H). (I) Stick diagram of the RGD loop bound to  $\alpha 5\beta 1$  crystal structure (PDB code 4WK4). The C $\beta$ -C $\beta$  distances between R6 and D8 in C, G, E, H, and R and D in I are shown. See also Figure S3.



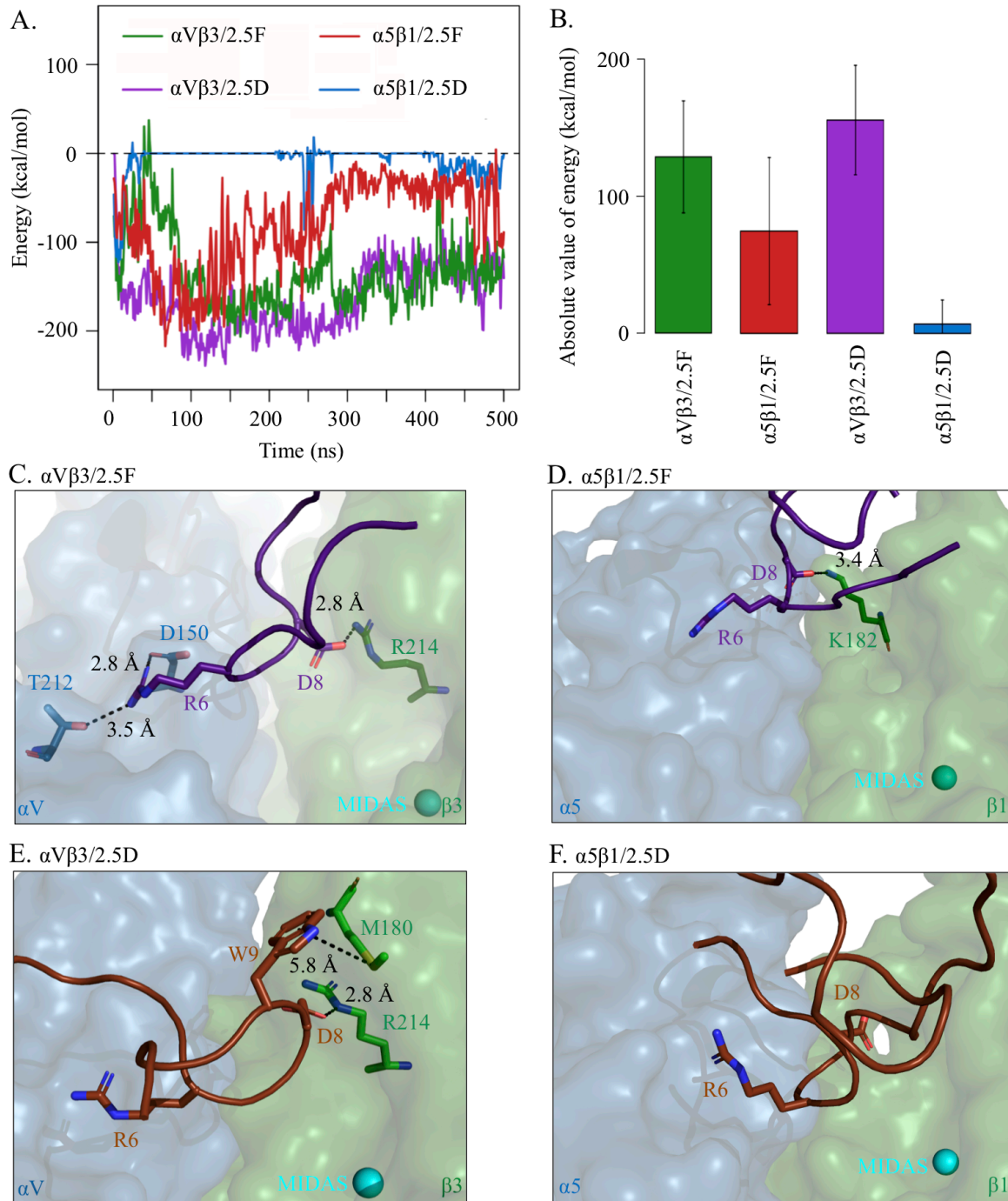


**Figure 5. MD simulations of 2.5D/2.5F binding to  $\alpha V\beta 3/\alpha 5\beta 1$ .** Knottins were initially separated by 9Å. (A) Energy over time and (B) bar graph (mean $\pm$  SD) showing absolute value of binding energies between 2.5D and 2.5F to  $\alpha V\beta 3$  and  $\alpha 5\beta 1$  averaged over 500 ns of simulation time. Difference between 2.5D/ $\alpha 5\beta 1$  and 2.5D/ $\alpha V\beta 3$ , 2.5F/ $\alpha V\beta 3$ , 2.5F/ $\alpha 5\beta 1$  is significant at  $p < 2.2 \times 10^{-16}$ . (C, D) Selected residues in structures of MD simulation of 2.5F binding to  $\alpha V\beta 3$  at t=0.020 ns (C) and to  $\alpha 5\beta 1$  at t=1.250 ns (D). (E, F) Selected residues in structures of MD simulation of 2.5D binding to  $\alpha V\beta 3$  at t=0.960 ns (E), and to  $\alpha 5\beta 1$  at t=1.250 ns (F). Distances (dotted lines) are indicated. The head segment of the respective integrin is displayed. See also Supplemental Movie 1, 2, 3 and 4.

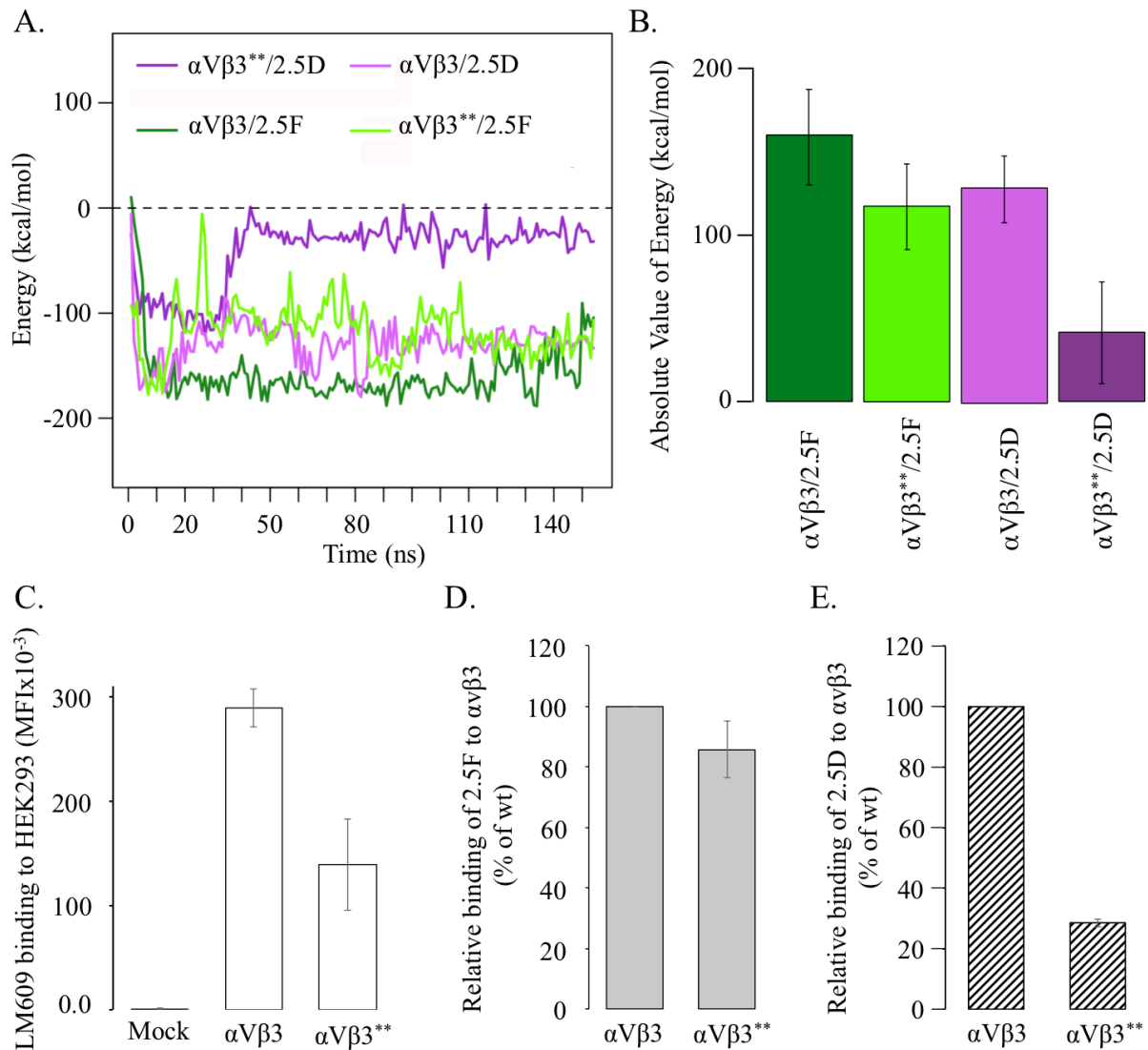


**Figure 6. Interaction of 2.5D and 2.5F with wild type and mutant  $\alpha V\beta 3$ .** (A) MD simulations of 2.5D and 2.5F binding to wild type (WT)  $\alpha V\beta 3$  and  $\alpha V\beta 3^{**}$  double mutant ( $\beta 3$ -M180A and  $\beta 3$ -R214G) showing energy over 160 ns. (B) Histograms showing values (mean  $\pm$  SD) of absolute energies from panel (A). Differences between  $\alpha V\beta 3/2.5D$  and  $\alpha V\beta 3^{**}/2.5D$  and between  $\alpha V\beta 3/2.5F$  and  $\alpha V\beta 3^{**}/2.5F$  were significant at p values of  $p < 2.2 \times 10^{-16}$  and  $1.9 \times 10^{-6}$ , respectively. (C-E) Histograms (mean  $\pm$  SD, n=4 independent experiments) showing binding of integrin antibody or Alexa 647-labelled 2.5F or 2.5D (each at 65 nM) to transiently transfected HEK293T- $\alpha V\beta 3$  and double mutant  $\beta 3$ -M180A and  $\beta 3$ -R214G  $\alpha V\beta 3^{**}$  in 1 mM  $Ca^{2+}/Mg^{2+}$  as determined by FACS analysis. (C) Binding of  $\alpha V\beta 3$  heterodimer specific antibody LM609 detected by APC-labeled goat anti-mouse Fc-specific antibody. (D) Binding of Alexa647-2.5F to  $\alpha V\beta 3$  and  $\alpha V\beta 3^{**}$ . (E) Binding of Alexa647-2.5D to  $\alpha V\beta 3$  and  $\alpha V\beta 3^{**}$ . Binding of the knottin to wild-type  $\alpha V\beta 3$  in D and E for each experiment was set to 100%. No differences are seen in binding of 2.5F to WT or  $\alpha V\beta 3^{**}$  ( $p > 0.05$ ) vs. 2.5D binding to the integrins ( $p = 7.6 \times 10^{-8}$ ).

## LEAD CONTACT AND MATERIALS AVAILABILITY

Further information and requests for resources and reagents should be directed to and will be fulfilled by the lead contact, M. Amin Arnaout (aarnaout1@mgh.harvard.edu).

## METHODS

**Peptide Synthesis.** Knottins 2.5D, 2.5F and the scrambled FN-RDG2 (where RGD motif is replaced with RDG) were prepared as previously described (Kimura et al., 2009b). Briefly, the linear 33-amino acid peptides starting with Gly1 (Figure 1A) were made by solid-phase peptide synthesis on a CS Bio (Menlo Park, CA) instrument using standard 9-fluorenylmethyloxycarbonyl chemistry. Knottin peptides were folded by promoting disulfide bond formation in oxidizing buffer at room temperature with gentle rocking overnight. Folded knottins were purified by reversed-phase HPLC, where they appeared as a sharp peak with a shorter retention time than unfolded or misfolded precursors. The molecular masses of folded knottins were determined by matrix-assisted laser desorption/ionization time-of-flight (MALDI-TOF) mass spectrometry (Stanford Protein and Nucleic Acid Facility). Folded 2.5F and 2.5D (2 mg/mL) were incubated with an amine-reactive succinimidyl ester derivative of Alexa Fluor 647 carboxylic acid in 0.1 M Hepes, pH 8.0, at a 5:1 dye/peptide molar ratio for 1 h at room temperature and then at 4 °C overnight. The free dye was removed by dialysis and buffer exchange into phosphate buffered saline (PBS).

**Plasmids, mutagenesis, protein expression and purification.** Human  $\alpha$ V $\beta$ 3 ectodomain was expressed in insect cells and purified as described (Mehta et al., 1998). The genetic sequence for knottins 2.5F, 2.5D or FN-RDG2 starting with Gly1 and ending with Gly33 (Figure 1A) was fused to the fragment crystallizable (Fc) region of mouse IgG2a in the pADD2 shuttle vector as described (Moore et al., 2013). The knottin Fc fusion proteins were expressed in human embryonic kidney (HEK293) cells following the manufacturer's protocols in the FreeStyle MAX 293 Expression System (Invitrogen). Secreted knottin-Fc fusion proteins were purified using Protein A Sepharose (Sigma) followed by size exclusion chromatography (Superdex 75 column; GE Life Sciences). Purified knottin-Fc fusion proteins were bivalent homo-dimers of the expected molecular weight of ~60 kDa (Moore et al., 2013).

**Mammalian Cell lines.** U87MG glioblastoma cells, K562 leukemia cells, and HEK293T embryonic kidney cells were obtained from American Type Culture Collection (Manassas, VA); integrin-transfected K562 cells (Blystone et al., 1994) were provided by Scott Blystone (SUNY Upstate Medical University).

**Binding assays.** 2.5D-Fc and 2.5F-Fc fusions were labeled with the succinimidyl ester derivative of Alexa Fluor 488 (Invitrogen) according to the manufacturer's protocol. Free dye was removed by dialysis and buffer exchange into PBS. U87MG cells were detached using Enzyme-Free Cell Dissociation Buffer (Gibco); K562 cells were grown in suspension.  $4 \times 10^4$  cells then incubated with varying concentrations (0.01 – 500 nM) of Alexa Fluor 488 labeled 2.5D- or 2.5F-Fc fusion proteins in 25 mM Tris pH 7.4, 150 mM NaCl, 2 mM CaCl<sub>2</sub>, 1 mM MgCl<sub>2</sub>, 1 mM MnCl<sub>2</sub>, and 0.1% bovine serum albumin (BSA) for 3 hours at 4 °C, to minimize internalization. Cells were pelleted and washed twice with 800  $\mu$ L of PBSA (phosphate buffered saline containing 0.1% bovine serum albumin) and the fluorescence of remaining surface-bound protein was measured

using flow cytometry using a Guava EasyCyte 8HT instrument (EMD Millipore). Raw data were processed using FlowJo software (TreeStar Inc.).

Wild type  $\alpha V\beta 3$  and mutated  $\alpha V\beta 3^{**}$  transiently transfected HEK293T cells were gently trypsinized and washed in DPBS buffer. Cells were re-suspended in complete culture medium, incubated for one hour at 37°C and subsequently washed in 1 mM  $Ca^{2+}/Mg^{2+}$ , 0.1% bovine serum albumin-supplemented Hepes buffered saline pH 7.4 (binding buffer).  $5 \times 10^6$  cells were incubated with Alexa647-labeled 2.5F or 2.5D (50 nM) in binding buffer for 30 min, at 25 °C then washed, re-suspended, fixed in 1% paraformaldehyde and analyzed by flow cytometry in a LSRII flow cytometer (BD). Anti- $\alpha V\beta 3$  antibody LM609 (20  $\mu g/ml$ ) was used to normalize  $\alpha V\beta 3$  cell surface expression in a separate set of tubes. Transfected HEK293T cells were stained with LM609 for 30 min at 4°C. After washing the excess antibody, APC-labeled goat anti-mouse Fc-specific antibody (10  $\mu g/ml$ ) was added for 30 min at 4°C, and the stained cells were washed, fixed and expression analyzed by flow cytometry as described above. Alexa-647 labeled knottin 2.5F or 2.5D binding to  $\alpha V\beta 3$  and  $\alpha V\beta 3^{**}$  was measured in mean fluorescence intensity (MFI) units, normalized according to LM609 binding and expressed as percentage of 2.5F or 2.5D binding to  $\alpha V\beta 3$ .

**NMR** A codon-optimized DNA sequence was prepared by assembly PCR and cloned into the pET-32 vector to express a protein product in *E. coli* containing a thioredoxin and His-tag fusion protein separated by a TEV protease site. Uniform  $^{15}N$ - and  $^{13}C$ -labeling was achieved by IPTG-induced expression in BL21-DE3 cells in M9 minimal media containing  $^{15}NH_4Cl$  and  $^{13}C$ -glucose. Cell lysis was followed by initial purification by His-tag capture with Ni-NTA. The thioredoxin fusion protein portion was removed with TEV protease to provide the exact 33-residue peptide sequence. Disulfide bond formation to fold the peptides was performed using the previously reported redox buffer (Kimura et al., 2009b). Final purification by RP-HPLC and characterization by ESI mass spectrometry confirmed folded engineered EETI-II peptides. NMR samples were prepared using sodium phosphate buffer, pH 6 containing 10%  $D_2O$ . Standard multidimensional NMR datasets were acquired for backbone and side chain resonance assignments, along with  $^{13}C$  (aliphatic and aromatic) and  $^{15}N$  3D-NOESY datasets for NOE-derived distance restraints. Dihedral angle restraints were derived from backbone assignments using TALOS+. 3D structure calculations were performed using the CYANA automated NOE assignment and simulated annealing algorithms. Initial structures calculated using standard automated NOE assignments led to convergence of 20 lowest energy structures, which were consistent with the expected knottin disulfide pattern. Further improved 3D structures were calculated by including disulfide bond restraints and hydrogen bond restraints determined by cross-hydrogen bond scalar couplings identified from long-range HNCO datasets. Final structures were refined by restrained molecular dynamics in explicit solvent using the YASARA package.

**Crystallography, structure determination and refinement.** The  $\alpha V\beta 3$  ectodomain was crystallized at 4 °C by vapor diffusion using the hanging drop method as previously described (Xiong et al., 2009; Xiong et al., 2001; Xiong et al., 2002). Knottins 2.5F or 2.5D (5 mM) was soaked into  $\alpha V\beta 3$  crystals in the crystallization well solution containing 1 mM  $Mn^{2+}$  for 2–3 weeks. Crystals were harvested in 12% PEG 3500 (polyethylene glycol, molecular weight 3500) in 100 mM sodium acetate, pH 4.5, 800 mM NaCl plus 2 mM  $Mn^{2+}$  and 2.5F or 2.5D (at 5 mM), cryoprotected by the addition of glycerol in 2% increments up to a 24% final concentration and

then flash frozen in liquid nitrogen. Diffraction data from cryo-cooled crystals were collected on the ID19 beamline fitted with a CCD detector at the APS Facility (Chicago, IL). Data were indexed, integrated and scaled with the HKL2000 (Otwinowski and Minor, 1997) program. Phases were determined by molecular replacement using PHASER (McCoy et al., 2007), with the structures  $\alpha_V\beta_3$  ectodomain (PDB ID 4MMX). Composite simulated annealing omit maps were then generated using the program Phenix Composite Omit Map package by turning on the simulated Cartesian annealing option with a temperature of 5,000K. The knottin structure was traced by the extra density using PDB 2IT7 and introducing the engineered mutations using Coot (Emsley and Cowtan, 2004). The resulting models were refined with the 1.10.1 version of Phenix (Adams et al., 2010) using simulated annealing, TLS, positional and individual temperature-factor refinement and default restraints. Several cycles of refinement and model building using Coot were applied to refine the structures of  $\alpha_V\beta_3/2.5D$ ,  $\alpha_V\beta_3/2.5F$  (Table 2), with automatic optimization of X-ray and stereochemistry and additional Ramachandran restraints in the last cycles. A-weighted  $2fo-fc$  electron density map was generated from the final models and structure factors using Phenix. All structural illustrations were prepared with the PyMol software (Schrödinger).

**Docking and Initial Configurations.** The NMR structures of 2.5F (PDB: 6MM4) and 2.5D (PDB ID: 2M7T) were docked onto the crystal structures of the integrin  $\alpha_V\beta_3$  (PDB ID: 4MMZ) and  $\alpha_5\beta_1$  (PDB ID: 4WJK) headpieces using the expert interface of the HADDOCK webserver. Four HADDOCK docking runs, between integrin  $\alpha_5\beta_1$  and 2.5D, integrin  $\alpha_5\beta_1$  and 2.5F, integrin  $\alpha_V\beta_3$  and 2.5D, and integrin  $\alpha_V\beta_3$  and 2.5F were performed. As docking inputs, the RGD sequence was specified as the active site of 2.5D and 2.5F. Residues  $\alpha_5$ -Glu<sup>221</sup>,  $\alpha_5$ -Asp<sup>227</sup>, and Mg<sup>2+</sup> ion at the MIDAS site were specified as the active site of integrin  $\alpha_5\beta_1$ , while residues  $\alpha_V$ -Asp<sup>150</sup>,  $\alpha_V$ -D<sup>218</sup>, and the MIDAS Mn<sup>2+</sup> ion, were specified as the active site of integrin  $\alpha_V\beta_3$ . To preserve the ion coordination of the MIDAS, ADMIDAS, and LIMBS ions during the docking run, unambiguous distance restraints between the coordinating groups and the MIDAS, ADMIDAS, and LIMBS ions were fed into HADDOCK. Furthermore, integrins  $\alpha_V\beta_3$  and  $\alpha_5\beta_1$  were specified as non-flexible in HADDOCK to prevent integrin backbone movement during docking. The RGD sequence of the knottins were specified as semi-flexible, while the non-RGD sequence was specified as non-flexible. Upon completion of the docking runs, the top solution from each generated cluster was analyzed. The best solution was then selected from these solutions based on maximal engagement of the specified active site residues.

**Molecular Dynamics Simulations** To simulate the interaction of 2.5D and 2.5F with integrins  $\alpha_V\beta_3$  and  $\alpha_5\beta_1$ , we performed Molecular Dynamics simulations using the top solution from each of the four HADDOCK structures. To setup the separated simulations, the axis between the center of mass of the integrin  $\beta_A$  domain and the knottin variants was determined in the four HADDOCK complexes. Knottin was then separated from the integrin by 9Å along this axis, allowing water molecules to populate the space in between the knottin and the integrin upon solvation of the structure. We also performed equilibration simulations on the available crystal structures of  $\alpha_V\beta_3$  in complex with 2.5D and 2.5F to be used as references. All structures were solvated and then ionized at a combined KCl concentration of 0.15 M. Structures were subsequently minimized for 100,000 steps and equilibrated for 0.5 ns using the NAMD molecular dynamics package (Phillips et al., 2005) and CHARMM27 force field (Brooks et al., 2009). Upon minimization, each of the four generated complexes ran for 500 ns. All simulations

ran at an initial temperature of 310 K using the Nose-Hoover thermostat, and pressure was maintained at 1 atm using the Langevin piston. All equilibration and production run simulations were performed using a time step of 2 fs. Electrostatics of the system were determined using the Particle mesh Ewald (PME) method. van der Waals (VDW) interactions were modeled using a switching function to smoothly reduce the VDW force to zero at the cutoff distance of 1.2 nm. Simulations were then analyzed using Visual Molecular Dynamics (VMD) (Humphrey et al., 1996).

**Accession numbers.** Coordinates for the NMR structures of knottins 2.5D and 2.5F and the crystal structures of  $\alpha\text{V}\beta\text{3}/2.5\text{D}$  and  $\alpha\text{V}\beta\text{3}/2.5\text{F}$  have been deposited in the PDB with ID codes 2M7T, 6MM4, 6MSL and 6MSU, respectively.

## EXPERIMENTAL MODEL AND SUBJECT DETAILS

Human glioblastoma cells (U87MG) were cultured in Dulbecco's Modified Eagle Medium (DMEM) supplemented with 10% Fetal Bovine Serum (FBS) and 1% penicillin-streptomycin (P/S). K562 leukemia cells were grown in liquid culture in IMEM Iscove's Modified Dulbecco's Medium (IMDM) supplemented with 10% FBS and 1% P/S. Human embryonic kidney cells (HEK293T) were cultured in DMEM supplemented with 10% FCS, 2 mM l-glutamine, 1 mM sodium pyruvate, penicillin, and streptomycin, and were transiently co-transfected with pcDNA3 plasmids encoding full-length wild-type  $\alpha\text{V}\beta\text{3}$ ,  $\alpha\text{V}\beta\text{3}^{**}$  ( $\alpha\text{V}\beta\text{3}$  with  $\beta\text{3-M180A}$  and  $\beta\text{3-R214G}$ ) using Lipofectamine 2000 reagent (Invitrogen) according to the manufacturer's protocol. 2.5D and 2.5F used for NMR structures were expressed in *E.coli* BL21 (DE3) cells grown in M9 minimal media containing  $^{15}\text{NH}_4\text{Cl}$  and  $^{13}\text{C}$ -glucose.

## QUANTITATION AND STATISTICAL ANALYSIS

Equilibrium dissociation constants ( $K_d$ ) for the binding data shown in Figures 1B and 1C were determined in SigmaPlot (Systat Software, San Jose, CA) using a least-square fit to a logistic curve. The standard error (SE) for  $K_d$  and t and p values were calculated using the reduced  $\chi^2$  method in SigmaPlot. The validity of the  $K_d$  value was assessed with a p value cutoff of 0.05. In Fig. 2C, RMSD was calculated between the C $\alpha$ 's in the different conformers and presented as mean $\pm$ SD in Fig. 2D. In Fig. 5B, the mean of the absolute values of the energies displayed in Fig. 5A are presented as histograms  $\pm$  SE. p values were calculated with the Student's t-test. In Fig. 6B, histograms derived from MD simulations of absolute energies shown in (A) are plotted  $\pm$  SD, with p values calculated by the Student's t-test. In Fig. 6 C-E, values represent mean  $\pm$ SD. p values were calculated with the Student's t-test.

## DATA AND SOFTWARE AVAILABILITY

All software and libraries used are reported in the Method Details section, together with the Key Resources Table. Coordinates for the NMR structures of knottins 2.5D and 2.5F and the crystal structures of  $\alpha\text{V}\beta\text{3}/2.5\text{D}$  and  $\alpha\text{V}\beta\text{3}/2.5\text{F}$  have been deposited in the PDB with ID codes 2M7T, 6MM4, 6MSL and 6MSU, respectively.

## References

- Adams, P.D., Afonine, P.V., Bunkoczi, G., Chen, V.B., Davis, I.W., Echols, N., Headd, J.J., Hung, L.W., Kapral, G.J., Grosse-Kunstleve, R.W., *et al.* (2010). PHENIX: a comprehensive Python-based system for macromolecular structure solution. *Acta Crystallogr D Biol Crystallogr* *66*, 213-221.
- Arnaout, M.A., Goodman, S.L., and Xiong, J.P. (2007). Structure and mechanics of integrin-based cell adhesion. *Curr Opin Cell Biol* *19*, 495-507.
- Blystone, S.D., Graham, I.L., Lindberg, F.P., and Brown, E.J. (1994). Integrin alpha v beta 3 differentially regulates adhesive and phagocytic functions of the fibronectin receptor alpha 5 beta 1. *J Cell Biol* *127*, 1129-1137.
- Bogdanowich-Knipp, S.J., Jois, D.S., and Siahaan, T.J. (1999). The effect of conformation on the solution stability of linear vs. cyclic RGD peptides. *J Pept Res* *53*, 523-529.
- Brooks, B.R., Brooks, C.L., 3rd, Mackerell, A.D., Jr., Nilsson, L., Petrella, R.J., Roux, B., Won, Y., Archontis, G., Bartels, C., Boresch, S., *et al.* (2009). CHARMM: the biomolecular simulation program. *J Comput Chem* *30*, 1545-1614.
- Caswell, P.T., Chan, M., Lindsay, A.J., McCaffrey, M.W., Boettiger, D., and Norman, J.C. (2008). Rab-coupling protein coordinates recycling of alpha5beta1 integrin and EGFR1 to promote cell migration in 3D microenvironments. *J Cell Biol* *183*, 143-155.
- Christoforides, C., Rainero, E., Brown, K.K., Norman, J.C., and Toker, A. (2012). PKD controls alphavbeta3 integrin recycling and tumor cell invasive migration through its substrate Rabaptin-5. *Dev Cell* *23*, 560-572.
- Coller, B.S., and Shattil, S.J. (2008). The GPIIb/IIIa (integrin alphaIIb beta3) odyssey: a technology-driven saga of a receptor with twists, turns, and even a bend. *Blood* *112*, 3011-3025.
- Dumont, R.A., Hildebrandt, I., Su, H., Haubner, R., Reischl, G., Czernin, J.G., Mischel, P.S., and Weber, W.A. (2009). Noninvasive imaging of alphaVbeta3 function as a predictor of the antimigratory and antiproliferative effects of dasatinib. *Cancer Res* *69*, 3173-3179.
- Emsley, P., and Cowtan, K. (2004). Coot: model-building tools for molecular graphics. *Acta Crystallogr D Biol Crystallogr* *60*, 2126-2132.
- Friedland, J.C., Lee, M.H., and Boettiger, D. (2009). Mechanically activated integrin switch controls alpha5beta1 function. *Science* *323*, 642-644.
- Guntert, P., Mumenthaler, C., and Wuthrich, K. (1997). Torsion angle dynamics for NMR structure calculation with the new program DYANA. *J Mol Biol* *273*, 283-298.
- Gupta, V., Gylling, A., Alonso, J.L., Sugimori, T., Ianakiev, P., Xiong, J.P., and Arnaout, M.A. (2007). The beta-tail domain (betaTD) regulates physiologic ligand binding to integrin CD11b/CD18. *Blood* *109*, 3513-3520.
- Hatley, R.J.D., Macdonald, S.J.F., Slack, R.J., Le, J., Ludbrook, S.B., and Lukey, P.T. (2018). An alphav-RGD Integrin Inhibitor Toolbox: Drug Discovery Insight, Challenges and Opportunities. *Angew Chem Int Ed Engl* *57*, 3298-3321.
- Humphrey, W., Dalke, A., and Schulten, K. (1996). VMD: visual molecular dynamics. *J Mol Graph* *14*, 33-38, 27-38.
- Kapp, T.G., Rechenmacher, F., Neubauer, S., Maltsev, O.V., Cavalcanti-Adam, E.A., Zarka, R., Reuning, U., Notni, J., Wester, H.J., Mas-Moruno, C., *et al.* (2017). A Comprehensive Evaluation of the Activity and Selectivity Profile of Ligands for RGD-binding Integrins. *Sci Rep* *7*, 39805.

- Kimura, R.H., Cheng, Z., Gambhir, S.S., and Cochran, J.R. (2009a). Engineered knottin peptides: a new class of agents for imaging integrin expression in living subjects. *Cancer Res* *69*, 2435-2442.
- Kimura, R.H., Levin, A.M., Cochran, F.V., and Cochran, J.R. (2009b). Engineered cystine knot peptides that bind  $\alpha v \beta 3$ ,  $\alpha v \beta 5$ , and  $\alpha 5 \beta 1$  integrins with low-nanomolar affinity. *Proteins* *77*, 359-369.
- Krieger, F., Moglich, A., and Kiefhaber, T. (2005). Effect of proline and glycine residues on dynamics and barriers of loop formation in polypeptide chains. *J Am Chem Soc* *127*, 3346-3352.
- Kryshtafovych, A., Moulton, J., Bales, P., Bazan, J.F., Biasini, M., Burgin, A., Chen, C., Cochran, F.V., Craig, T.K., Das, R., *et al.* (2014). Challenging the state of the art in protein structure prediction: Highlights of experimental target structures for the 10th Critical Assessment of Techniques for Protein Structure Prediction Experiment CASP10. *Proteins* *82 Suppl 2*, 26-42.
- Kwan, B.H., Zhu, E.F., Tzeng, A., Sugito, H.R., Eltahir, A.A., Ma, B., Delaney, M.K., Murphy, P.A., Kauke, M.J., Angelini, A., *et al.* (2017). Integrin-targeted cancer immunotherapy elicits protective adaptive immune responses. *J Exp Med* *214*, 1679-1690.
- Mason, W.P. (2015). End of the road: confounding results of the CORE trial terminate the arduous journey of cilengitide for glioblastoma. *Neuro Oncol* *17*, 634-635.
- McCoy, A.J., Grosse-Kunstleve, R.W., Adams, P.D., Winn, M.D., Storoni, L.C., and Read, R.J. (2007). Phaser crystallographic software. *J Appl Crystallogr* *40*, 658-674.
- Mehta, R.J., Diefenbach, B., Brown, A., Cullen, E., Jonczyk, A., Gussow, D., Luckenbach, G.A., and Goodman, S.L. (1998). Transmembrane-truncated  $\alpha v \beta 3$  integrin retains high affinity for ligand binding: evidence for an 'inside-out' suppressor? *Biochem J* *330 (Pt 2)*, 861-869.
- Moore, S.J., Hayden Gephart, M.G., Bergen, J.M., Su, Y.S., Rayburn, H., Scott, M.P., and Cochran, J.R. (2013). Engineered knottin peptide enables noninvasive optical imaging of intracranial medulloblastoma. *Proc Natl Acad Sci U S A* *110*, 14598-14603.
- Nero, T.L., Morton, C.J., Holien, J.K., Wielens, J., and Parker, M.W. (2014). Oncogenic protein interfaces: small molecules, big challenges. *Nat Rev Cancer* *14*, 248-262.
- Otwinowski, Z., and Minor, W. (1997). Processing of X-ray diffraction data collected in oscillation mode. *Methods Enzymol* *276*, 307-326.
- Pabon, N.A., and Camacho, C.J. (2017). Probing protein flexibility reveals a mechanism for selective promiscuity. *Elife* *6*.
- Park, H.S., Kim, C., and Kang, Y.K. (2002). Preferred conformations of RGD tetrapeptides to inhibit the binding of fibrinogen to platelets. *Biopolymers* *63*, 298-313.
- Phillips, J.C., Braun, R., Wang, W., Gumbart, J., Tajkhorshid, E., Villa, E., Chipot, C., Skeel, R.D., Kale, L., and Schulten, K. (2005). Scalable molecular dynamics with NAMD. *J Comput Chem* *26*, 1781-1802.
- Raab-Westphal, S., Marshall, J.F., and Goodman, S.L. (2017). Integrins as Therapeutic Targets: Successes and Cancers. *Cancers (Basel)* *9*.
- Reynolds, A.R., Hart, I.R., Watson, A.R., Welti, J.C., Silva, R.G., Robinson, S.D., Da Violante, G., Gourlaouen, M., Salih, M., Jones, M.C., *et al.* (2009). Stimulation of tumor growth and angiogenesis by low concentrations of RGD-mimetic integrin inhibitors. *Nat Med* *15*, 392-400.

- Ruoslahti, E., and Pierschbacher, M.D. (1987). New perspectives in cell adhesion: RGD and integrins. *Science* 238, 491-497.
- Sheldrake, H.M., and Patterson, L.H. (2014). Strategies to inhibit tumor associated integrin receptors: rationale for dual and multi-antagonists. *J Med Chem* 57, 6301-6315.
- Shen, Y., Delaglio, F., Cornilescu, G., and Bax, A. (2009). TALOS+: a hybrid method for predicting protein backbone torsion angles from NMR chemical shifts. *J Biomol NMR* 44, 213-223.
- Takada, Y., Ye, X., and Simon, S. (2007). The integrins. *Genome Biol* 8, 215.
- Van Agthoven, J.F., Xiong, J.P., Alonso, J.L., Rui, X., Adair, B.D., Goodman, S.L., and Arnaout, M.A. (2014). Structural basis for pure antagonism of integrin alphaVbeta3 by a high-affinity form of fibronectin. *Nat Struct Mol Biol* 21, 383-388.
- Wilson, I.A., and Stanfield, R.L. (1994). Antibody-antigen interactions: new structures and new conformational changes. *Curr Opin Struct Biol* 4, 857-867.
- Xiong, J.P., Mahalingham, B., Alonso, J.L., Borrelli, L.A., Rui, X., Anand, S., Hyman, B.T., Rysiok, T., Muller-Pompalla, D., Goodman, S.L., *et al.* (2009). Crystal structure of the complete integrin alphaVbeta3 ectodomain plus an alpha/beta transmembrane fragment. *J Cell Biol* 186, 589-600.
- Xiong, J.P., Stehle, T., Diefenbach, B., Zhang, R., Dunker, R., Scott, D.L., Joachimiak, A., Goodman, S.L., and Arnaout, M.A. (2001). Crystal structure of the extracellular segment of integrin alpha Vbeta3. *Science* 294, 339-345.
- Xiong, J.P., Stehle, T., Zhang, R., Joachimiak, A., Frech, M., Goodman, S.L., and Arnaout, M.A. (2002). Crystal structure of the extracellular segment of integrin alpha Vbeta3 in complex with an Arg-Gly-Asp ligand. *Science* 296, 151-155.